Multiple Transients in the Pre-Steady-State of Nucleoside Hydrolase Reveal Complex Substrate Binding, Product Base Release, and Two Apparent Rates of Chemistry†

An Vandemeulebroucke, Wim Versées, Jan Steyaert, and John N. Barlow*

Department of Ultrastructure, Vlaams Interuniversitair Instituut voor Biotechnologie, Vrije Universiteit Brussel, Pleinlaan 2, 1050 Brussel, Belgium

Received April 5, 2006; Revised Manuscript Received May 22, 2006

ABSTRACT: We have investigated the transient kinetics of the nucleoside hydrolase from *Trypanosoma vivax* (*Tv*NH) at low temperatures (5 °C). Three novel absorbance transients (termed τ1, τ3, and τ4) were detected during multiple-guanosine turnover stopped-flow absorbance spectroscopy, in addition to a transient (τ2) that had been observed previously at 35 °C. At 5 °C, *Tv*NH displays full-sites activity and not half-of-the-sites activity as is apparent at 35 °C. Both τ1 and τ2 are assigned to chemistry based on rapid-quench results. For τ1, the rate of chemistry is ca. 3000-fold faster than k_{cat} (1−2 orders of magnitude greater than previous estimates). The pH dependencies of the burst amplitudes for τ1 and τ2 indicate that these transients arise from the formation of two different dimeric *Tv*NH·substrate complexes and not from *Tv*NH that contains kinetically asymmetric monomers. The saturating burst rates for τ1 and τ2 are surprisingly pH-independent, given the prominent role of acid−base chemistry in the proposed mechanism for *Tv*NH. τ3 and τ4 are assigned to the substrate binding and base release processes, respectively, and shown to be equivalent to two fluorescence transients (τ3* and τ4*, respectively) observed previously by stopped-flow methods at 35 °C. The rate of base release is shown to be an apparent rate. Together with steady-state product inhibition results, the data indicate that *Tv*NH follows an ordered uni-bi kinetic mechanism with a *Tv*NH·base dead-end complex, and not the rapid equilibrium random uni-bi mechanism proposed for other NHs. Two applicable kinetic models are presented and their implications for future mechanistic studies discussed.

N-Glycosidic bond cleavage is an important reaction found in a variety of cellular contexts, including DNA repair (via the action of DNA glycosylases), cell poisoning (via ribosylation agents such as the cholera toxin), and in purine salvage pathways [via the action of nucleoside phosphorylases and nucleoside hydrolases, (*1*−*3*)]. *N*-Glycosidic bonds are kinetically very stable [the $t_{1/2}$ for nucleoside hydrolysis is on the order of 1000 years at pH 7.0 and 25 °C (*4*)], and therefore, substantial catalytic power is required to make this reaction physiologically useful.[1] For example, nucleoside hydrolases (NHs,[2] Scheme 1) that enhance the rate of nucleoside hydrolysis by factors of at least 10^{12} (*6*) using mechanisms which are not yet completely understood have evolved (*7*, *8*). To gain a better understanding of NH catalytic mechanisms, we have been pursuing structural and mechanistic studies of the purine-specific NH from *Trypanosoma vivax* (*Tv*NH).

Scheme 1: *N*-Glycosidic Bond Cleavage

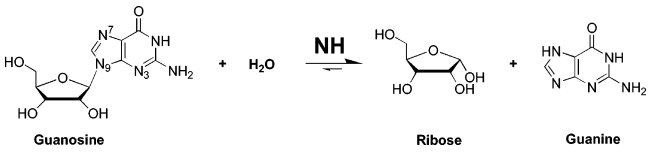

Kinetic isotope effect studies indicate that the reactant transition-state structures for nonenzymatic and NH-catalyzed nucleoside hydrolysis are similar (*9*, *10*). In these structures, the ribosyl moiety of the nucleoside has substantial oxocarbenium ion character as a result of the *N*-glyocosidic bond being almost fully broken, with only weak bonding interactions to the incoming water nucleophile. Three chemical strategies have been invoked to explain how NH avoids paying ca. 17.7 kcal/mol in transition-state energy (*11*): (i) distortion and electrostatic stabilization of the ribosyl group to promote ribooxocarbenium ion formation, (ii) activation and strategic positioning of the substrate water to capture the ribooxocarbenium ion at the transition state (TS), and (iii) purine leaving group (LG) activation by protonation or hydrogen bonding. The observation of a high degree of

† This work was supported in part by the Vlaams Interuniversitair Instituut voor Biotechnologie. A.V. was supported by a grant from Institute for the Promotion of Innovation through Science and Technology in Flanders (IWT-Vlaanderen). W.V. was supported by a grant from the FWO-Vlaanderen.

* To whom correspondence should be addressed. Telephone: +32-2-6291846. Fax: +32-2-6291963. E-mail: jbarlow@vub.ac.be.

[1] Spontaneous *N*-glycosidic bond hydrolysis in DNA occurs at a significant rate with profound physiological consequences (*5*).

[2] Abbreviations: NH, nucleoside hydrolase; *Tv*NH, nucleoside hydrolase from *Trypanosoma vivax*; *Cf*NH, nucleoside hydrolase from *Crithidia fasciculata*; *Tbb*NH, nucleoside hydrolase from *Trypanosoma brucei brucei*; TS, transition state; LG, leaving group; pNPR, *p*-nitrophenyl riboside; ImmH, immucillin H or (1*S*)-1-(9-deazahypoxanthin-9-yl)-1,4-dideoxy-1,4-imino-D-ribitol; PzImmH, 8-aza-immucillin H or (1*S*)-1-(7-hydroxy-1*H*-pyrazolo[4,3-*d*]pyrimidin-3-yl)-1,4-dideoxy-1,4-imino-D-ribitol; τ, transient.

10.1021/bi060666r CCC: $33.50
Published on Web 07/04/2006

structural conservation between different NHs in the region of the active site that makes bonding interactions with the ribosyl moiety and substrate water suggests that the first two strategies are conserved (*12*−*14*).

As purine and pyrimidine nucleosides exhibit considerably different acid−base properties, resulting in a much greater sensitivity toward specific-acid catalysis for purine nucleosides (*1*, *15*−*17*), it may be anticipated that the LG activation process is intimately related to the substrate specificity displayed by an NH. Indeed, LG activation is thought to play a minor role in the IU−NH (base-aspecific) from *Crithidia fasciculata* (*Cf*NH) (*8*) which hydrolyzes purine and pyrimidine nucleosides with similar proficiencies (*18*, *19*). For example, removal of the general acid likely responsible for N-7 protonation (His 241) in *Cf*NH by mutagenesis resulted in a 2100-fold drop in k_{cat} for inosine with respect to that of the wild type (*20*); the H241A mutant is still an impressive catalyst, however, with a rate enhancement of ca. 10^9-fold relative to that of solution solvolysis.

In contrast, inhibitor and substrate structure−activity studies in purine-specific NHs suggest that LG activation, via general acid catalysis and/or other electrostatic interactions, plays a much more prominent catalytic role (*11*, *13*, *21*, *22*). For example, the substrate analogue *p*-nitrophenyl riboside (pNPR), which lacks the pyrimidine and purine ring nitrogens as proton acceptors in specific acid-catalyzed solvolysis, is a poor substrate for purine-specific NHs but a good one for base-aspecific NHs. Structural comparisons of the active sites of purine and base-aspecific NHs have also revealed significant structural differences in the active site region that interacts with the purine LG (*13*, *23*). For the purine-specific NH from *T. vivax*, the LG in the *Tv*NH·substrate complex is stacked in an anti conformation between two tryptophan side chains (Trp 83 and Trp 260, which correspond to Ile 81 and His 241, respectively, in *Cf*NH). A recently published structure of *Tv*NH (*24*) in complex with the transition-state analogue inhibitor immucillin-H (ImmH), in which electron density for the entire active site was observed for the first time, shows only two hydrogen bonding interactions between the enzyme and the purine: N-3 of the purine with Asp 40 and O-6 of the purine with Arg 252. However, removal of these hydrogen bond interactions by mutagenesis failed to induce significant changes in the steady-state kinetic parameters k_{cat} and k_{cat}/K_m for nucleoside hydrolysis. Thus, there does not appear to be a role for direct LG activation in *Tv*NH by either hydrogen bonding or general acid catalysis.

Instead, a novel mechanism in which the arene−arene stacking interaction between Trp 260 and the purine LG substantially increases the pK_a at N-7 has been proposed, facilitating its protonation by solvent (*25*). This mechanism is supported by mutagenesis experiments and computational calculations and also by the recent *Tv*NH·ImmH structure which shows that a channel of tightly bound water molecules (with low *B* factors) leads from bulk solvent to both N-7 and N-1 of ImmH (*24*). Recently, substrate-assisted catalysis has been proposed as an additional mechanism for leaving group activation via hydrogen bond formation between the C′-5 hydroxyl group and C-8 hydrogen of the purine leaving group (*26*).

Interpretations of the effects of mutagenesis on *Tv*NH activity (including chemistry) based on steady-state parameters k_{cat} and k_{cat}/K_m are, however, limited and potentially misleading. This is because the rate-determining step in the hydrolytic direction is product ribose release (*27*), and the extent to which chemistry limits k_{cat}/K_m is unknown. We have therefore embarked on a detailed examination of the transient kinetics of *Tv*NH with the aim of directly measuring the rates of chemistry and other events (e.g., active site loop movement) to facilitate interpretation of mutagenesis data and estimate the importance of LG activation. Previous multiturnover stopped-flow studies at 35 °C identified a monophasic decay absorbance transient[3] that was assigned to the *N*-glycosidic bond cleavage step, with an amplitude that corresponded to half-of-the-sites activity (*27*). Two fluorescence transients (decay rise) were also observed by stopped-flow spectroscopic measurement of *Tv*NH tryptophan fluorescence during multiple turnovers. These were assigned to substrate binding and to the conversion of the Michaelis complex to the *Tv*NH·ribose product complex, respectively. Fluorescence transients were also observed in binding experiments with substrate (biphasic decay, attributed to a two-step binding process) and ribose (monophasic decay, also attributed to two-step binding on the basis of the concentration dependence). Here, we examine the transient kinetics of *Tv*NH at 5 °C and at different pH's. The progress curves are considerably richer in information than those previously reported at 35 °C and indicate that the *Tv*NH reaction pathway is more complex than anticipated.

MATERIALS AND METHODS

General Procedures. The concentrations of enzyme, nucleoside, and purine stock solutions were determined using the following extinction coefficients (*29*): $\epsilon_{280} = 47.75$ mM^{-1} cm^{-1} for *Tv*NH (pH 7.0), $\epsilon_{253} = 13.6$ mM^{-1} cm^{-1} for guanosine (pH 6.0), $\epsilon_{248.5} = 12.3$ mM^{-1} cm^{-1} for inosine (pH 6.0), $\epsilon_{276} = 8.15$ mM^{-1} cm^{-1} for guanine (pH 7.0), and $\epsilon_{249.5} = 10.7$ mM^{-1} cm^{-1} for hypoxanthine (pH 6.0). Nucleosides and purine solutions were made fresh on the day of use in deionized water, except for guanine which was made up in 40 mM NaOH. Once thawed, *Tv*NH stocks (>200 μM) were kept at 4 °C and used over a period of several days but not refrozen to avoid activity loss. *Tv*NH activity loss was apparent during storage on ice over several hours in dilute samples (<1 μM).

Expression, Purification, and Mass Analysis of TvNH. *Tv*NH was purified as described previously (*13*) with the exception that an imidiazole gradient (10−500 mM over 10 column volumes at pH 8) was used instead of a pH gradient to elute bound protein off the Ni affinity column. The purity of *Tv*NH was estimated to be >95% from visual inspection of Coomassie-stained SDS−PAGE gels. Sample integrity was determined by electrospray mass spectrometry (ESI-MS): a single major ion species (observed mass of 37 584.6 Da with MaxEnt data processing; predicted average isotopic mass of 37 583.96 Da) was observed. Partial loss of the N-terminal His tag and the presence of a 16 Da ion peak as a result of N-terminal methionine oxidation (verified by peptide mapping, results not shown) were evident in some *Tv*NH batches. To verify that the biphasic transients observed

[3] A term of the form $Ae^{-\lambda t}$ in the fitted absorbance time course, where A is the amplitude, λ is the rate constant, and t is the time (*28*).

by stopped-flow absorbance did not originate from post-translational modification of the N-terminal His tag, we expressed and purified recombinant *Tv*NH that lacked the N-terminal His tag (*Tv*NH-B). *Tv*NH-B was homogeneous as determined by ESI-MS (observed mass of 36 185.6 Da; predicted average isotopic mass with loss of N-terminal methionine of 36 185.48 Da) and gave progress curves identical to that of *Tv*NH which contained the N-terminal His tag.

Product Inhibition Studies. Steady-state product inhibition studies were performed at 25 °C in potassium phosphate (50 mM, pH 7.0, ionic strength adjusted to 200 mM with NaCl) with *p*-nitrophenyl riboside (pNPR) as a substrate ($\Delta\epsilon_{400}$ = 12 mM^{-1} cm^{-1}, K_m = 230 μM). Assays were initiated by adding *Tv*NH (final concentration of 100 nM) to a solution containing pNPR (50−500 μM) and variable concentrations of either ribose (0.35−5.5 mM) or hypoxanthine (50−400 μM). Hypoxanthine was chosen instead of guanine because of its greater solubility. Data were analyzed using both linear plots [Dixon and Lineweaver Burk plots (*30*)] and by direct nonlinear fitting using Dynafit (*31*). The model discrimination analysis feature of Dynafit, in which simulated velocity data for competitive, uncompetitive, and mixed-type inhibition mechanisms are fitted to the observed velocity data, was used to select the best inhibition model. All three approaches gave essentially the same results. The values obtained from the direct fits are reported in the Results.

Stopped-Flow General Procedures. Stopped-flow analysis was performed on an Applied Photophysics model SX18.MV stopped-flow spectrofluorimeter fitted with a xenon lamp. Mixing efficiency was tested using phenol red in the absorption mode (*32*). The dead time of the instrument (2 ms) was determined using the procedure of Tonomura et al. (*33*) with total drive volumes of 160 μL. Progress curves were collected in oversampling mode with logarithmic time bases and auto-offset to permit the signal range to be optimized. Transients were recorded for >5 times the relaxation time; 10 s time bases were sufficient to permit accurate determination of steady-state rates. All experiments were performed under pseudo-first-order conditions with a minimally 4-fold excess of substrate over *Tv*NH. All reported concentrations are final concentrations in the reaction mixture.

Stopped-Flow Absorbance. Multiple turnovers of guanosine and inosine by *Tv*NH was followed by stopped-flow absorbance. The photomultiplier (PM) voltage corresponding to zero absorbance was set using water in the observation cell (1 cm path length). The instrumental signal-to-noise ratio for absorbance measurements was 1 mAU, and all progress curves had a maximum absorbance of <1. All solutions were made in buffer (50 mM, ionic strength of 200 mM with NaCl). Progress curves were averaged (generally 10−14 shots) and corrected for background signal changes by subtracting the averaged progress curve for a sample containing substrate only. Changes in molar extinction ($\Delta\epsilon$'s) for nucleoside hydrolysis were determined by measuring the total absorbance change during complete nucleoside hydrolysis in situ. Exploratory progress curves were measured across the wavelength range of 250−300 nm at 5 nm intervals to detect novel transients.

Stopped-Flow Fluorescence. Changes in *Tv*NH fluorescence during multiple-substrate turnover and during ligand binding were measured with excitation at 280 nm and detection above 305 nm, using a 305 nm cutoff filter. The PM voltage was set at 80% of full scale with *Tv*NH at the working concentration in buffer, with a path length of 0.2 cm. Progress curves were averaged (typically 5−10 shots) and corrected for background signal changes by subtracting a control (*Tv*NH only) progress curve. The fluorescence intensity response was linear up to 5 μM *Tv*NH. The working concentration of *Tv*NH was fixed at 0.5−1 μM.

Stopped-Flow Data Analysis (28). Linear and nonlinear curve fitting to progress curves was performed using Microsoft Origin version 7. The first 2 ms of the progress curves was discarded. Goodness of fit was estimated by inspection of residuals. The fitting functions had the general form (eq 1):

$$y(t) = \sum_i A_i \exp(-k_i t) + \upsilon t + C \quad (1)$$

where $y(t)$ is the observed signal at time t, i is the number of transients, A_i is the amplitude of the ith transient, k_i is the observed rate constant (k_{obs}) for the ith transient, ν is the steady-state velocity, and C is the offset. The fitted parameters were used to make plots of observed rate constants and amplitudes versus substrate, base, or ribose concentrations. Linear data (τ3, τ3*, and guanine binding) were fitted to eq 2:

$$k_{obs} = k_{on}[L] + k_{off} \quad (2)$$

where [L] is the ligand concentration. Ribose binding data were analyzed as described previously (*27*). Hyperbolic fits were made using eq 3:

$$k_{obs} = \frac{k_{sat}[L]}{K_m' + [L]} \quad (3)$$

The meanings of fitted parameters k_{on}, k_{off}, k_{sat}, and K_m' are discussed in the Results.

pH Dependency of Transient Kinetics. All kinetic experiments were performed in 50 mM buffer at a constant ionic strength (200 mM, adjusted with NaCl). Buffer inhibition was apparent in both steady-state and transient kinetic measurements with amine-containing buffers (HEPES, TAPS, and Tris) in the pH range of 7−9. For example, the observed rate constants for τ1 and τ2 decreased by ca. 50% with an increase in the HEPES concentration from 12.5 to 100 mM at pH 7.0, while there was little change in the observed burst amplitudes. No buffer inhibition was observed with phosphate which was therefore used in the pH range of 6.2−9.0. Changes in pH due to the weak buffering capacity of phosphate at pH 9.0 were not observed. Piperazine (50 mM) was used at pH 5.5 and 6.2 and potassium acetate (50 mM) at pH 4.5. Plots of observed amplitude for τ1 and τ2 versus H^+ concentration were made for the pH 7.0−9.0 data and fitted according to eq 4 (*34*):

$$A_H = \frac{P_1[H^+] + P_2K_a}{K_a + [H^+]} \quad (4)$$

where A_H is the observed amplitude, P_1 is the high-H^+

concentration asymptote, P_2 is the low-H^+ concentration asymptote, and K_a is the apparent acid dissociation constant.

Rapid Quench. Rapid-quench measurements were performed to follow the production of guanine in the *Tv*NH reaction at several pH's. Rapid quench was performed at 5 °C using a QFM-5 quench-flow apparatus (Bio-Logic). Delay-line volumes, minimal purge volumes, and maximal permitted flow rates were tested using protocols provided by the manufacturer. Correct sample volumes were verified by weighing. Precipitation of substrate nucleoside due to insolubility at high concentrations was checked by measuring the absorbance spectrum during storage on ice. Quenching was performed with 1 M HCl or 1 M NaOH, both giving essentially identical results. Overlapping delay times were used for each delay line that was used and between continuous and interrupted modes. In continuous mode, equal volumes of substrate, *Tv*NH, and quencher were driven to give a 1:1 ratio of substrate to *Tv*NH in the delay line and a 1:2 ratio of quencher to reaction mix in the quenched sample. The *Tv*NH concentration in the delay line was either 10 or 20 μM. Substrate concentrations in the delay line are as given in the Results. The final quencher concentration was 333 mM. Samples were kept on ice prior to filtration at 4 °C using wetted Microcon centrifugal device microconcentrators (YM-30, regenerated cellulose, 30 kDa cutoff, Amicon). The filtrates were neutralized using either acid or base, and the amount of guanine was quantified using reverse-phase HPLC as described previously (*13*) except that manual integration of the guanine peaks was performed at 266 nm. Both control A (quencher added to guanosine prior to *Tv*NH) and control B (quencher added to guanosine only) gave guanine peak areas essentially identical to that of control C (guanosine in water only). The guanine concentration was calculated using a guanine standard curve with eq 5:

$$[\text{guanine}] = \left(\frac{\text{area}_G - \text{area}_{CB}}{\text{slope}}\right) \times \text{DF} \qquad (5)$$

where area_G is the guanine peak area in the *Tv*NH sample, area_{CB} is the area of the guanine peak in control B, slope is the gradient of guanine standard curve (units of area per micromolar guanine), and DF is the dilution factor.

RESULTS

Multiple-Turnover Stopped-Flow Absorbance Spectroscopy at 5 °C and pH 8.0, Followed at 260 nm. Previous multiple-turnover stopped-flow absorbance experiments on *Tv*NH were carried out at 35 °C, with detection of guanosine hydrolysis at 260 nm (*27*). As the transient kinetics of *Tv*NH are fast at 35 °C, we performed all experiments here at 5 °C to obtain more accurate data and identify novel transients that were occurring too rapidly at higher temperatures. Indeed, the observed absorbance burst with guanosine as the substrate was biphasic at 5 °C, in contrast to the monophasic burst previously observed at 35 °C (Figure 1). At pH 8.0 and 5 °C, the two transients [τ1 (fast) and τ2 (slow)] have equal amplitudes (Figure 2a), the total amplitude corresponding to full-sites activity (confirmed by rapid quench; see below). The observed burst rate dependencies on guanosine concentration for both τ1 and τ2 show saturation behavior (Figure 2b), permitting maximal burst rates for the two transients to be estimated: saturating k_{obs} (τ1) = 121 ± 15 s^{-1}; saturating k_{obs} (τ2) = 12.16 ± 0.72 s^{-1}. Notably, the apparent rate of chemistry for τ1 is ca. 3000-fold faster than the rate of product ribose release (k_{cat} = 0.038 s^{-1}) under saturating conditions.

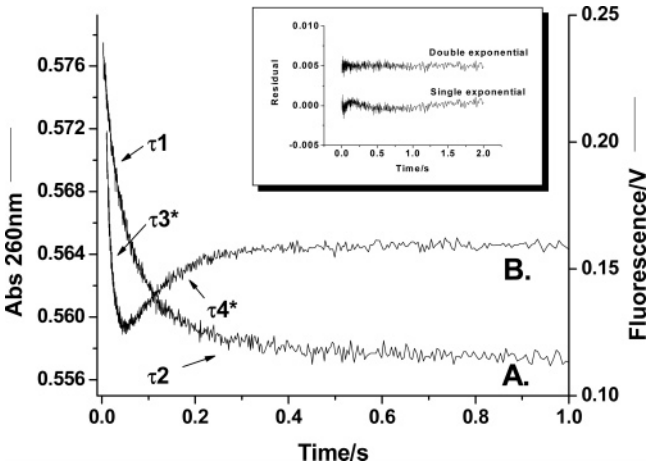

FIGURE 1: Stopped-flow absorbance (A) and fluorescence (B) progress curves of *Tv*NH (5 μM monomer for panel A and 0.5 μM monomer for panel B) with 50 μM guanosine at pH 8. The inset shows residuals from single- and double-exponential fittings of the absorbance curve. The residual for the double-exponential fit is shown with a +0.005 AU offset for clarity.

Multiple-Turnover Stopped-Flow Absorbance Spectroscopy at 5 °C and pH 8.0, with Detection at Wavelengths where $\Delta\epsilon = 0$. Two new transients (τ3 and τ4, Figure 3) were also detected during multiple-substrate (guanosine) turnover stopped-flow absorbance spectroscopy at 280 nm, at which wavelength the change in extinction coefficient ($\Delta\epsilon$) upon *N*-glycosidic bond hydrolysis is approximately zero. The substrate concentration dependencies of the observed rate constants for τ3 and τ4 are identical to those of the two fluorescence transients previously observed during multiple-substrate turnover (*27*) and are here termed τ3* and τ4*, respectively (Figure 1). The linear dependencies on substrate concentration for τ3 and τ3* indicate that they both originated from the substrate binding step, while the saturation behavior of τ4 and τ4* shows that these transients arise from a process after the binding step (shown for the fluorescence transients in Figure 2b). Furthermore, the rate constants of τ4 and τ4* also match those of τ2 (but not at pH 7; see below).

Multiple-Turnover Stopped-Flow Absorbance Spectroscopy with Inosine as the Substrate. The physical origin of the changes in optical properties during τ4 and τ4* was examined using inosine as the substrate. Inosine displays essentially the same steady-state (*13*) and transient rate constants as guanosine. Transients corresponding to τ3/τ3* and τ4/τ4* were observed in multiple-turnover stopped-flow absorbance experiments with 268 nm detection (where $\Delta\epsilon$ for inosine hydrolysis is approximately zero). However, the observed amplitudes of τ3 and τ4 with inosine are opposite in sign from those observed with guanosine (Figure 3). To exclude the possibility that the amplitude change arose from different detection wavelengths, we compared the two progress curves at the same wavelength (275 nm). At this wavelength, absorbance changes from *N*-glycosidic bond cleavage also contribute to the progress curves, making detection of τ4 for inosine difficult (Figure 4). However, the difference in the observed amplitude for τ3 between inosine

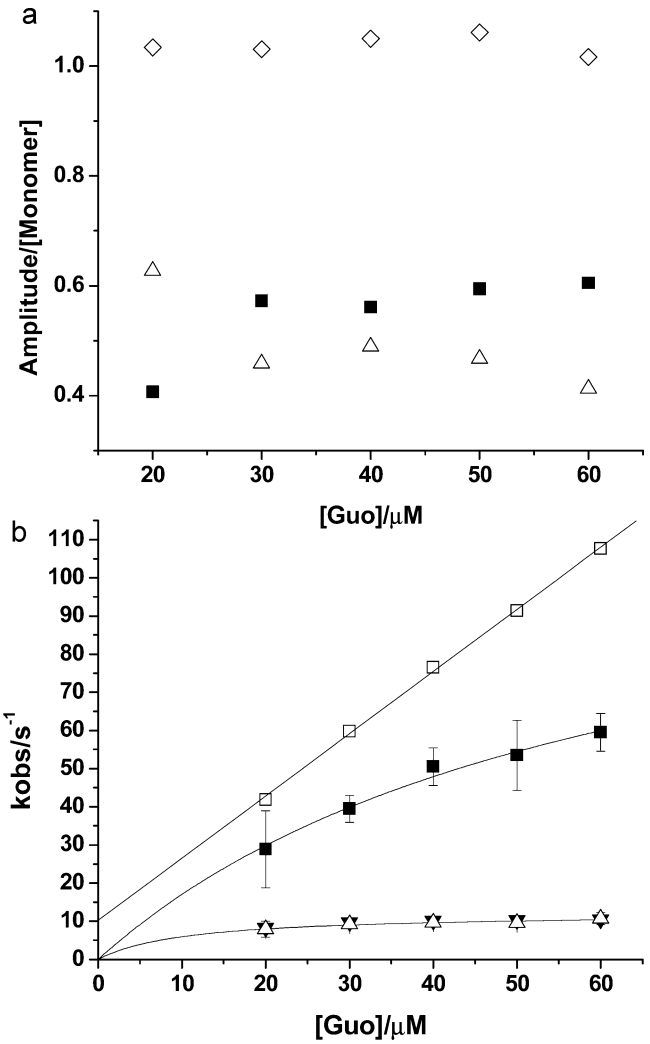

FIGURE 2: (a) Plot of burst amplitudes vs substrate concentration (20−60 μM) from a single multiple-turnover stopped-flow absorbance experiment at pH 8.0 and 5 μM *Tv*NH monomer. Amplitudes of τ1 (■), τ2 (△), and the sum of τ1 + τ2 (◇) are shown. (b) Plot of observed burst rates (k_{obs}) vs substrate concentration (20−60 μM) at pH 8.0. The enzyme concentrations used were 5 μM (for absorbance measurements) and 0.5 μM (for fluorescence measurements). The rate constants of τ1 (■), τ2 (△), τ3* (□), and τ4* (▼) are shown. Error bars shown on τ1 and τ2 refer to the standard deviation from two separate experiments. Linear (τ3*) and hyperbolic fits (τ1, τ2, and τ4*) are also shown.

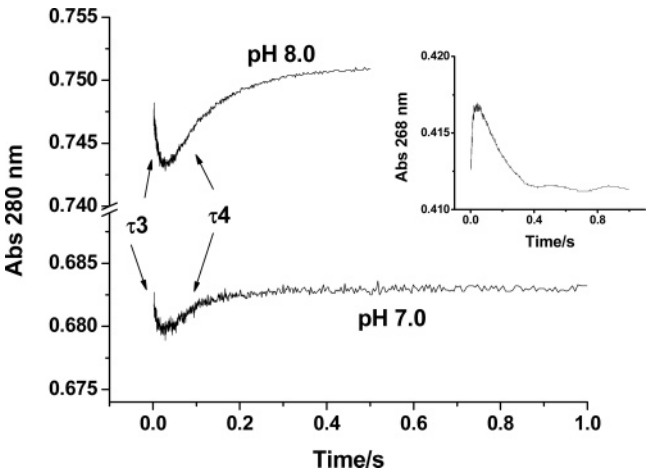

FIGURE 3: Stopped-flow absorbance progress curves for guanosine (50 μM) turnover by *Tv*NH (5 μM) at pH 7.0 and 8.0 with detection at 280 nm. The inset shows stopped-flow absorbance progress curves for inosine (50 μM) turnover by *Tv*NH (5 μM) at pH 7.0 with detection at 268 nm.

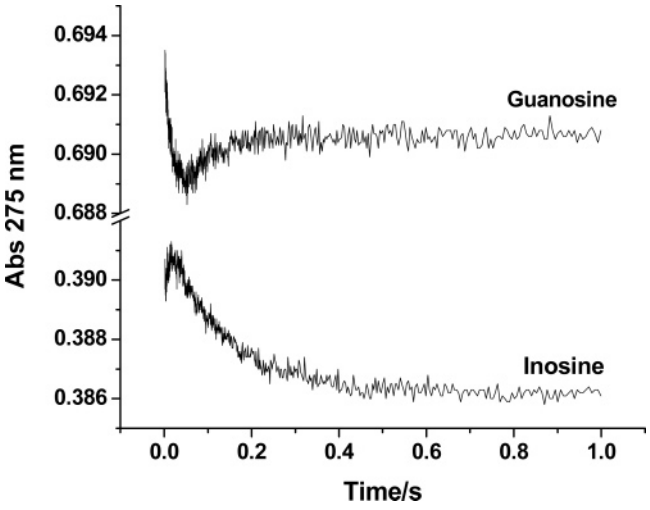

FIGURE 4: Stopped-flow absorbance of guanosine (50 μM) and inosine (50 μM) turnover by *Tv*NH (5 μM) at pH 7.0 with detection at 275 nm. On the basis of the measured $\Delta\epsilon$'s for nucleoside hydrolysis (both <0; chemistry gives absorbance decrease), essentially no chemistry contributes to the guanosine progress curve, while chemistry dominates the absorbance decay for inosine.

and guanosine is still apparent. The transients observed during binding of guanine and hypoxanthine to free *Tv*NH also display amplitudes of opposite signs (data not shown). We conclude from this dependency of the absorption amplitude on the chemical nature of the purine LG that direct interactions between the purine moiety of the nucleoside and active site residues Trp 83 and Trp 260 are responsible for the changes in optical properties during τ3 and τ4. Furthermore, the observation that the amplitude of τ4 is equal in magnitude but opposite in sign to that of binding transient τ3 (for both guanosine and inosine), and the observation that there is a restoration of fluorescence intensity during τ4* (in contrast to the fluorescence quenching observed during substrate or base binding; see below) strongly indicates that the changes in optical properties that take place during τ4 and τ4* are caused by purine LG release.

Steady-State and Pre-Steady-State Measurements of Base Binding. Binding of guanine to free *Tv*NH also gives rise to a monophasic fluorescence decay transient in stopped-flow experiments (data not shown). A plot of k_{obs} versus guanine concentration is linear with a slope k_{on} of 3.33 ± 0.47 μM^{-1} s^{-1} and a *y*-intercept k_{off} of 110 ± 28 s^{-1}, giving a dissociation constant K_d of 33 μM. The decay transient has an amplitude similar in magnitude to that of τ3* but significantly larger (ca. 2-fold) than that observed during ribose binding. Attempts were also made to detect binding of guanine to the preformed *Tv*NH·ribose binary complex by stopped-flow fluorescence. In principle, three fluorescence transients should be observable when the *Tv*NH·ribose binary complex is mixed with guanine if ternary complex formation takes place (as there are three coupled equilibria, corresponding to formation of *Tv*NH·ribose, *Tv*NH·guanine, and *Tv*NH·ribose·guanine complexes). However, only two fluorescence transients are observed, with amplitudes and rate constants consistent with formation of the binary complexes only (data not shown).

We postulated that the absence of a third binding transient may be caused by weak binding of guanine to the *Tv*NH·ribose complex. As only low concentrations of guanine (<0.1 mM) could be used in the stopped-flow experiments (to maintain the sample absorbance at <1), we carried out product inhibition experiments under steady-state turnover conditions with hypoxanthine at high concentrations to determine the affinity of purine for the *Tv*NH·ribose complex. Significant formation of the *Tv*NH·ribose·hypoxanthine ternary complex was predicted to generate a mixed inhibition profile. However, both ribose and hypoxanthine only show slope linear competitive patterns using pNPR as a substrate (K_{is} for hypoxanthine = 136 μM, K_{is} for ribose = 1.0 mM). In the presence of 10 mM ribose, the apparent K_{is} for hypoxanthine increases to 600 μM, but no evidence of mixed inhibition was detected. This pattern is consistent with an ordered uni-bi mechanism in which hypoxanthine forms a dead-end complex (giving rise to slope linear competitive inhibition) but only binds to the *Tv*NH·ribose complex weakly.

pH Dependencies of the Transients Observed with Multiple-Turnover Stopped-Flow Absorbance Spectroscopy with 260 nm Detection at 5 °C. In view of the postulated importance of LG activation in the *Tv*NH mechanism, and in particular the catalytic role of N-7 protonation, we also examined the pH dependency of the transient kinetics (Figure 5a,b). A biphasic burst is observed by stopped-flow absorbance at 260 nm throughout the pH range of 4.5−9.0. Surprisingly, the saturating rate constants for τ1 and τ2 show only small changes across these pH ranges (Figure 5a and Table 1). It should be noted that accurate estimates of the rate constant for τ1 above pH 8 are precluded by its small amplitude and interference from substrate binding absorbance changes. At pH 10, no burst is observed, possibly due to enzyme instability (the fluorescence spectrum is unstable at this pH), while at pH 3.0, a burst that has a small amplitude that could not be definitively assigned to chemistry is observed. The total burst amplitude is also relatively constant in the pH range of 4.5−9.0, but the relative amplitudes of τ1 and τ2 are reciprocally pH dependent (Figure 5b). The region between pH 7.0 and 9.0 is especially interesting because the relative amplitudes of τ1 and τ2 appear to follow the titration profiles of a single group with an apparent pK_a of 8.0.

pH Dependencies of the Transients Observed with Multiple-Turnover Stopped-Flow Fluorescence Spectroscopy at 5 °C. For τ3*, there is little change in the observed rate constants in the pH range of 7.0−9.0 (Table 1). Plots of k_{obs} versus guanosine concentration at different pH's display similar slopes (k_{on}, guanosine association rate constant) and *y*-axis intercepts [k_{off}, guanosine dissociation rate constant if the steady-state level of the *Tv*NH·guanosine complex is reached sufficiently rapidly; otherwise, it includes rate constant terms from subsequent steps (*28*)]. At pH 5.5 and 6.2, however, the initial fluorescence decay observed in the progress curves is biphasic, and the two transients are labeled τ3*(a) and τ3*(b). Plots of k_{obs} versus guanosine concentration for both transients are linear functions of substrate concentration; however, the *y*-intercept for the second transient [τ3*(b)] is negative, possibly as a result of fitting errors.

The fluorescence recovery phase of the progress curve (τ4*) is monophasic throughout the pH range of 5.5−9.0. In the pH range of 7.0−9.0, the k_{obs} versus guanosine concentration profiles indicate a decrease in both the saturating rate (k_{sat}) and K_m' (guanosine concentration that gave the half-maximal k_{obs}) with an increase in pH (Table 1). Notably, the rate constant of τ4* is significantly greater than that of τ2 at pH 7.0 (but similar to or equal to that of τ2 at other pH's), indicating that τ2 and τ4* (and τ4) are actually different transients.

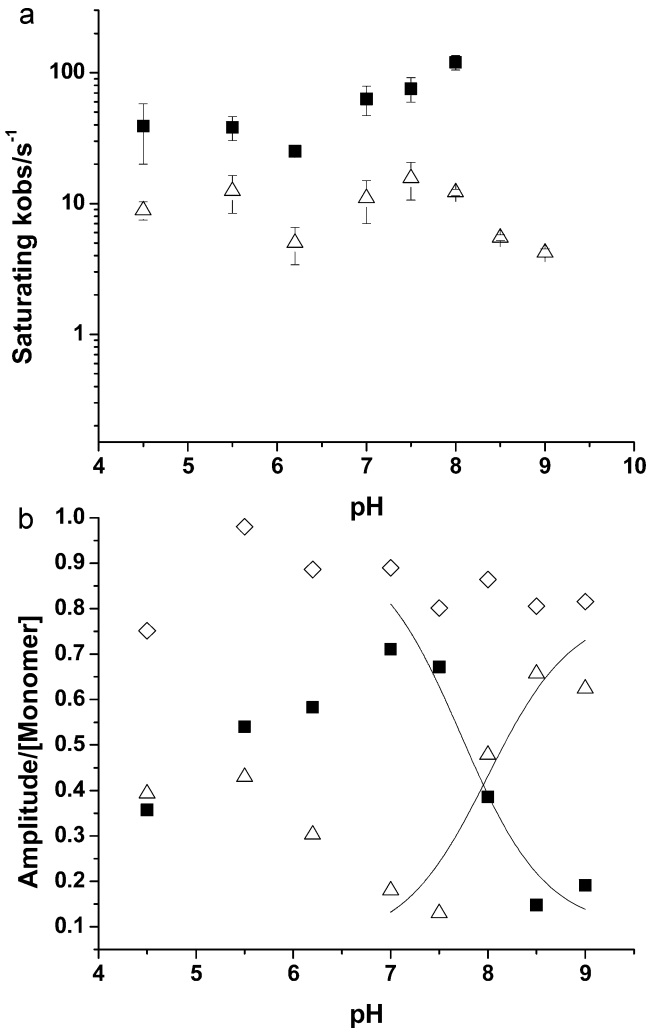

FIGURE 5: (a) pH dependencies of saturating burst rates for τ1 (■) and τ2 (△). The error bars represent the standard errors from nonlinear fitting. Plots of k_{obs} vs guanosine concentration for the pH 6.2, 8.5, and 9.0 data were flat. Therefore, the saturating k_{obs} was calculated as the mean value, with error bars representing the standard deviation. The rates for τ1 at pH 8.5 and 9 are not plotted because of interference from binding transients. The plotted rates of τ1 and τ2 at pH 6.2, 7.0, and 8.0 represent the mean of two experiments. (b) pH dependencies of burst amplitudes for τ1 (■), τ2 (△), and the sum of τ1 + τ2 (◇). Note that the data points for τ1 at pH 8.5 and 9 represent upper limits for the amplitudes, as a result of interference from the binding transient. Nonlinear fits of eq 4 (Materials and Methods) to the pH 7.0−9.0 data are also shown.

pH Dependency of Product Guanine Formation by Multiple-Turnover Rapid Quench at 5 °C. That the total absorbance burst amplitude (τ1 + τ2) originates primarily from chemistry, and not from absorbance changes arising from nonchemistry events, was confirmed by measuring the transient kinetics of product guanine formation by rapid quench at pH 7.0, 8.0, and 9.0 (Figure 6). The observed burst amplitude ([guanine]/[protein monomer]) is ca. 0.8 at each pH, in close agreement with that observed by stopped-flow methods.

Table 1: Fitted Parameters from Stopped-Flow Data[a]

	τ1	τ2	τ3*	τ4*		
pH	k_{sat} (s^{-1})	k_{sat} (s^{-1})	k_{on} (μM^{-1} s^{-1})	k_{off} (s^{-1})	k_{sat} (s^{-1})	K_m' (μM)
4.5	39 ± 19	8.9 ± 1.4	ND[d]	ND[d]	ND[d]	ND[d]
5.5	38.3 ± 8.4	12.4 ± 4.0	2.04 ± 0.22	80 ± 12	10.0 ± 1.6	185 ± 40
6.2	25.0 ± 1.4[b]	5.4 ± 1.6[b]	2.83 ± 0.17	41.6 ± 6.7	>5[e]	> 60[e]
7.0	63 ± 16[c]	10.5 ± 4.3[c]	1.09 ± 0.09	33.3 ± 4.8	25.3 ± 2.2	41.5 ± 8.0
7.5	75 ± 16	15.7 ± 4.7	ND[d]	ND[d]	ND[d]	ND[d]
8.0	120 ± 15[c]	12.16 ± 0.72[c]	1.630 ± 0.030	10.2 ± 1.3	12.11 ± 0.42	8.4 ± 1.5
8.5	ND[d]	5.47 ± 0.27[b]	1.497 ± 0.017	8.10 ± 0.87	4.471 ± 0.085[b]	ND[d]
9.0	ND[d]	4.28 ± 0.20[b]	1.002 ± 0.057	15.0 ± 4.4	1.87 ± 0.11[b]	ND[d]

[a] Unless stated, the standard error from linear or nonlinear curve fitting is shown. [b] Mean and standard deviation of data at different guanosine concentrations (k_{obs} vs guanosine concentration plot had a zero gradient). [c] Mean and standard error of two experiments. [d] Not determined. [e] Plot of k_{obs} vs guanosine concentration linear in the tested range (0−60 μM).

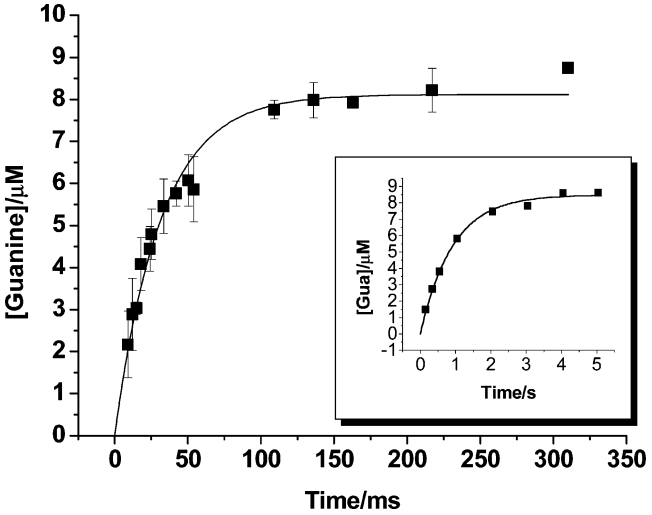

FIGURE 6: Guanine product formation by *Tv*NH (10 μM) during multiturnover of guanosine (100 μM), as followed by rapid quench at pH 7.0 and 9.0 (inset). The solid lines are single-exponential fits (k_{obs} = 35 s^{-1} for pH 7.0; k_{obs} = 1 s^{-1} for pH 9.0). The pH 7.0 data represent the mean of three experiments with standard deviation error bars.

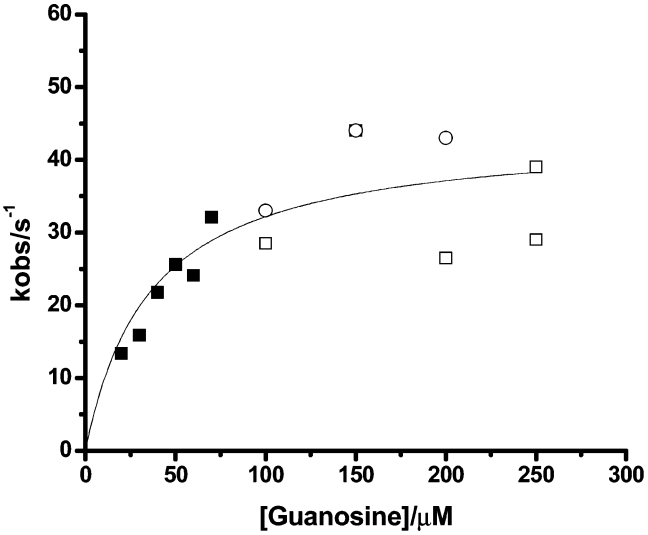

FIGURE 7: Combined stopped-flow and rapid-quench burst rate constants obtained at different guanosine concentrations (20−250 μM) at pH 7.0. Rate constants were determined using single-exponential fitting of the burst phase. The *Tv*NH concentration was 5 μM for the stopped-flow data and 10 μM for the rapid-quench data. Data for stopped flow (■), rapid quench with HCl quench (○), and rapid quench with NaOH quench (□) are shown. Also shown is a hyperbolic fit (—) with the following parameters: $k_{obs,max}$ = 43.8 ± 5.1 s^{-1} and K_m' = 36 ± 15 μM.

Direct confirmation of the rate constants and amplitudes for τ1 and τ2 by rapid quench was not possible because the data were not sufficiently accurate to permit double-exponential fitting and were therefore fitted to single-exponential functions. However, the rate constants thus obtained from rapid quench are consistent with those obtained by single-exponential fitting of the stopped-flow absorbance data (Figure 7). Furthermore, the observed rate constant from rapid quench at pH 9 is identical to that of τ2 (1 s^{-1}, at 100 μM guanosine in TAPS buffer), while at pH 7, the rate constants are much greater than τ2 but less than τ1 (rapid quench = 35 s^{-1} at 100 μM guanosine, predicted τ1 at 100 μM = 44 s^{-1}, predicted τ2 at 100 μM = 7 s^{-1}). Thus, the rapid-quench data are consistent with the interpretation that τ1 and τ2 are both chemistry transients that have pH-dependent amplitudes but pH-independent rate constants.

Scheme 2: One-Chemistry Step Kinetic Model for *Tv*NH

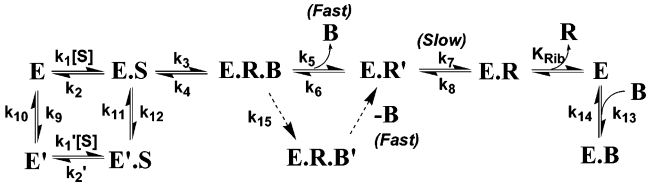

Scheme 3: Two-Chemistry Step Kinetic Model for *Tv*NH

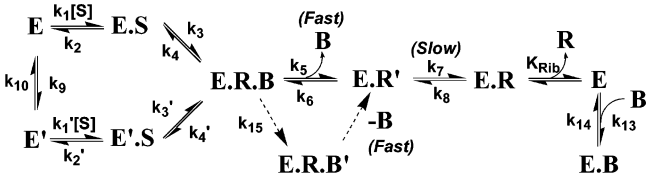

DISCUSSION

On the basis of these and previous results, we have proposed two possible schemes for the *Tv*NH reaction (Schemes 2 and 3 and Table 2). Both models are based on an ordered uni-bi kinetic mechanism with base release preceding ribose release and the formation of a dead-end *Tv*NH·base binary complex. They also show the formation of two *Tv*NH·substrate complexes, fast base dissociation, and two-step ribose release. Two pathways for base release are shown in each model. In one pathway, base release follows chemistry immediately. In the second pathway (indicated with dashed arrows), base dissociation is preceded by an isomerization step of the *Tv*NH·ribose·base ternary complex.

Table 2: Kinetic Constants for *Tv*NH, Using the Nomenclature of Schemes 2 and 3

	experimental evidence	pH 7	pH 9
k_1 (μM^{-1} s^{-1})	$\tau 3$*	1.24 ± 0.16	ND
k_2 (s^{-1})	$\tau 3$*	$<26.5 \pm 5.3$	ND
$k_3 + k_4$ (s^{-1})	$\tau 1$	82 ± 12	ND
$k_3' + k_4'$ (s^{-1})	$\tau 2$	8.5 ± 3.0	4.55 ± 0.34
k_5 (s^{-1})		>600	ND
k_6 (μM^{-1} s^{-1})		ND	ND
k_7 (s^{-1})	ribose binding	0.057 ± 0.031,[a] 0.04[b]	0.02[b]
k_8 (s^{-1})	ribose binding	21.29 ± 0.27	ND
K_{Rib} (mM)	ribose binding	67.2 ± 3.0	ND
k_9 (s^{-1})		ND	ND
k_{10} (s^{-1})		ND	ND
k_1' (μM^{-1} s^{-1})	$\tau 3$*	ND	1.002 ± 0.057
k_2' (s^{-1})	$\tau 3$*	ND	$<15.1 \pm 4.4$
$k_{11} + k_{12}$ (s^{-1})	$\tau 2$	8.5 ± 3.0	4.55 ± 0.34
k_{13} (μM^{-1} s^{-1})	guanine binding	3.33 ± 0.47	ND
k_{14} (s^{-1})	guanine binding	110 ± 28	ND
k_{15} (s^{-1})	$\tau 4$*[c]	25.3 ± 2.2	1.87 ± 0.11

[a] Determined from measurement of the extent of ribose binding by stopped-flow fluorescence at 5 °C. [b] Determined from measurement of the steady-state rate by stopped-flow absorbance at 260 nm. [c] This interpretation applies if the rate of base release is determined by an isomerization step after chemistry.

The isomerization of the *Tv*NH·ribose binary complex that precedes ribose dissociation is the overall rate-determining step in the hydrolytic direction. The two models differ in the catalytic competencies of the two *Tv*NH·substrate binary complexes that are formed initially. In the "one-chemistry step" model, only one of these binary complexes (E·S) undergoes chemistry. The other binary complex (E′·S) undergoes a slow isomerization to form the E·S binary complex before chemistry can take place. In the "two-chemistry step" model, both *Tv*NH·substrate binary complexes are catalytically competent. We justify these schemes below.

It should be noted that kinetic simulation programs, which are commonly used to analyze multiple progress curves (*35*), were of limited utility here. This was caused by several factors, such as rate constants for $\tau 1$ and $\tau 2$ that are comparable in magnitude, the absence of lag periods in the absorbance profiles (which we interpret as arising from binding transient interference), and large errors in the molar response coefficients for the fluorescence data (compounded by deviations in baseline and amplitude fluorescence intensities as a result of substrate absorbance and enzyme instability at low concentrations).

TvNH Follows an Ordered Uni-Bi Kinetic Mechanism. It has been established that both *Cf*NH and *Tbb*NH follow rapid equilibrium random uni-bi kinetic schemes (*18*, *22*, *36*). This conclusion is based on the observation of fully expressed kinetic isotope effects and the observed slope linear competitive product inhibition patterns for ribose and hypoxanthine. Competitive product inhibition (slope effect) arises in this case because addition of saturating amounts of substrate reduces the level of the *Tv*NH·ribose·hypoxanthine complex to zero (*37*). In other words, the conversion of the *Tv*NH·substrate complex to the *Tv*NH·ribose·hypoxanthine complex is slow compared to substrate and product binding and release steps. The binding steps therefore attain equilibrium during the steady state, and the K_m for the substrate is equal to its dissociation constant. However, the structural and kinetic evidence indicates that this model is not valid for *Tv*NH, even though slope linear competitive inhibition with ribose and hypoxanthine was also observed. First, the crystal structures of *Tv*NH in complex with substrate or inhibitor show that the ribose moiety is buried away from the bulk solvent by protein residues and the base itself. This makes establishment of a rapid equilibrium between the *Tv*NH·ribose·base and the *Tv*NH·base complexes unlikely. Second, our transient kinetics results show that ribose dissociation is preceded by a slow *Tv*NH·ribose isomerization step (k_7, Schemes 2 and 3) that is rate-determining overall and that base release precedes this isomerization step (k_5, Schemes 2 and 3). The separation of the ribose dissociation and base dissociation steps by a slow step prevents saturating levels of substrate from reducing the level of the *Tv*NH·ribose·base complex to zero (since finite concentrations of the *Tv*NH·ribose·base complex will be maintained if k_7 is small). Therefore, the absence of an observed intercept effect in the product inhibition experiments must arise because hypoxanthine binds weakly to the *Tv*NH·ribose binary complex. The increase in the apparent K_{is} for hypoxanthine upon inclusion of high concentrations of ribose can be attributed to the formation of a *Tv*NH·hypoxanthine dead-end complex [although the observed increase (0.6 mM) is slightly lower than that expected on the basis of pure competition (1.4 mM)].

TvNH Displays Two Chemistry Transients. The largest absorption difference between guanosine and guanine (in the detection range of the stopped-flow instrument) occurs at 260 nm. The observation of two transients at 260 nm during multiturnover stopped-flow absorbance with guanosine indicates that chemistry (*N*-glycosidic bond cleavage) occurs at two apparent rates. This interpretation is supported by the rapid-quench data, despite the two transients not being able to be resolved by this technique. First, the guanine burst amplitude observed by rapid quench matches the total absorbance burst amplitude ($\tau 1 + \tau 2$) in the pH range of 7.0−9.0 and corresponds to full-sites activity (Figures 5b and 6). Second, the rate constants from single-exponential fitting of the data collected with the two techniques match closely (Figure 7), consistent with this rate constant being a weighted average of those of $\tau 1$ and $\tau 2$ with the weightings depending on the relative amplitudes at that particular pH.[4]

The saturating rate constants for $\tau 1$ and $\tau 2$ represent lower limits for all the first-order rate constants that lead up to and include the chemistry step in the hydrolytic direction. Thus, the saturating rate may be determined by an isomerization step (e.g., a conformational change) that occurs before chemistry rather than chemistry itself. The observation of two rates of chemistry further implies that two different *Tv*NH·substrate complexes must form (E·S and E′·S in Schemes 2 and 3) and that interconversion between these two complexes must be slow compared to the rate of chemistry. In the one-chemistry step model (Scheme 2), two *Tv*NH·substrate complexes are formed initially, but only one (E·S) is catalytically competent and gives rise to chemistry

[4] An alternative explanation, that the biphasic pattern at 260 nm resulted from the superposition of a single chemistry transient with interfering binding ($\tau 3$) and base release ($\tau 4$) transients, was also considered but ruled out; see the Supporting Information.

(and the transient $\tau 1$, with rate constant $k_3 + k_4$). The E′·S complex undergoes a slow isomerization to form the E·S complex [at a relaxation rate ($k_{11} + k_{12}$), corresponding to $\tau 2$]. In the two-chemistry step model (Scheme 3), both $\tau 1$ and $\tau 2$ represent intrinsic chemistry rates that arise from the breakdown of two catalytically competent (Michaelis) *Tv*NH·substrate complexes (E·S and E′·S).

Both Schemes 2 and 3 show two forms of the free *Tv*NH (E and E′), although this is not necessary for the formation of two different *Tv*NH·substrate complexes. The existence of two different forms of free *Tv*NH is supported by the observation of two binding transients in the stopped-flow fluorescence progress curves at low pH. However, further experiments are needed to put this conclusion on a firmer footing because of the difficulty in fitting three exponential functions to the fluorescence progress curves. Biphasic fluorescence decay transients were also observed upon binding of guanosine to the catalytically inactive D10A *Tv*NH mutant but were assigned to a two-step binding mechanism because plots of the observed rate constants ($\tau 1 + \tau 2$) versus S concentration and $\tau 1\tau 2$ versus S concentration were linear (*27*).

The fast rate of chemistry ($\tau 1$ is ca. 3000 times faster than k_{cat}) has implications for the interpretation of the steady-state kinetics of *Tv*NH mutants. In contrast to that of the wild type, the saturating steady-state rates of mutants that display a reduced k_{cat} are potentially determined by chemistry. Thus, the 10-fold decreases in k_{cat} observed for the W260A mutant imply that the rate of chemistry is reduced by approximately 4−5 orders of magnitude compared to that of the wild type, 1−2 orders of magnitude more than previously estimated at 35 °C (*25*). On the other hand, the rate of chemistry may be reduced by up to 3 orders of magnitude in other mutants and not give rise to an observable change in k_{cat}.

Implications for Sites Activity. The discrepancy in the observed sites activity between 35 °C (half-of-the-sites) and 5 °C (full-sites) is likely due to $\tau 1$ reaching completion during the dead time of the stopped-flow instrument at 35 °C. Above 15 °C, the stopped-flow absorbance progress curves are well fitted to single-exponential functions. Arrhenius plots of the observed burst rates (not shown) indicate that $\tau 1$ is strongly temperature dependent, with a dependency similar to that of k_{cat} (4-fold increase in rate going from 5 to 15 °C). An alternative explanation for the change in sites activity is that the kinetic mechanism is modified by temperature. This explanation has yet to be tested. It should be noted that full-sites binding of the immucillin Pz-ImmH at 25 °C has been reported (*24*).

Interpretation of the Two TvNH·Substrate Binary Complexes. The burst amplitudes of $\tau 1$ and $\tau 2$ under saturating substrate concentrations represent the relative concentrations of the E·S and E′·S complexes, respectively, that form before significant chemistry has taken place. The amplitude pH dependencies make it unlikely that $\tau 1$ and $\tau 2$ originate from asymmetric *Tv*NH dimers (i.e., $\tau 1$ from monomer A and $\tau 2$ from monomer B of the same dimer) because the amplitude of each transient attains values greater than one-half the total monomer concentration. Instead, E·S and E′·S likely represent symmetrical dimers that differ in their protonation states, consistent with the observation of identical monomers in the crystal structure (*24*).

One plausible interpretation of the E·S and E′·S species is that one of these complexes contains the nucleoside in the syn conformation while the other complex has the nucleoside bound in the anti conformation. It should be reemphasized that the rate of interconversion between the two bound conformers must be slow compared to the rate of chemistry to generate two chemistry transients. For free nucleosides, interconversion between these two conformers takes place on the nanosecond time scale (*38*). The isomerization of nucleoside bound to *Tv*NH has been examined using molecular dynamics simulations, based on the 3-deazaadenosine-bound *Tv*NH crystal structure (*13*, *39*). These simulations indicated that the anti to syn conversion also takes place on the nanosecond time scale, with the syn conformer being the preferred ground-state conformation. However, the structural model used in these simulations differs significantly from that of the *Tv*NH−ImmH complex structure that was determined recently (*24*), especially the structure of active site loop 2 which had to be modeled in the simulation. Two of the three determined *Tv*NH crystal structures containing bound nucleoside display the anti conformation (*13*, *23*, *24*); furthermore, turnover of inosine in the anti conformation was observed in *Tv*NH(D10A)·inosine crystal complexes (*23*), indicating that the anti conformer is catalytically competent. Thus, both the rate of anti−syn isomerization of the bound nucleoside and the catalytic competence of the syn-bound form are still open questions.

Implications of the pH−Rate Profiles for the TvNH Catalytic Mechanism. The pH dependencies of the saturating burst rates for $\tau 1$ and $\tau 2$ provide more direct information about the pH dependence of chemistry than steady-state pH profiles, as they reflect the pH dependency of the *Tv*NH·substrate to *Tv*NH·ribose·base complex transformation. The k_{cat}−pH profile for *Tv*NH with natural purine nucleosides as substrates is not very informative because k_{cat} is a measure of the rate of the slow *Tv*NH·ribose complex isomerization step prior to ribose dissociation. The weak pH dependency of rates of $\tau 1$ and $\tau 2$ in the pH range of 4.5−8.0 is very similar to the k_{cat}/K_m−pH dependencies observed for both *Tv*NH (*23*) and the purine-specific NH from *Trypanosoma brucei brucei* [*Tbb*NH (*36*)]. As k_{cat}/K_m is a measure of the rate of productive binding (*40*), the weak pH dependencies shown by k_{cat}/K_m, and by both $\tau 1$ and $\tau 2$, indicate that neither binding (averaged over the two binding processes) nor chemistry is perturbed in this pH region. The drop in k_{cat}/K_m seen at high pH for *Tv*NH ($pK_a = 8.6$), *Tbb*NH ($pK_a = 8.6$), and *Cf*NH (9.1) is likely caused by ionization of N-1 of inosine [$pK_a = 8.76$ (*41*)]. This interpretation is supported by the observation that xanthosine, which exists primarily as the monoanion [pK_a(N-3) = 5.7 (*42*)], has an anomalously low k_{cat}/K_m compared to the other purine nucleosides at pH 7.0 (*23*). Ionization of the bound substrate may account for the small drop in rate for $\tau 2$ at high pH (pK_a of N-1 for free guanosine = 9.2; Figure 5a); however, the change in rate was smaller than that observed for k_{cat}/K_m, and an alternative explanation is that guanosine is sticky (*43*).

In view of the postulated importance of N-7 protonation for catalysis in *Tv*NH, and the predicted pK_a of ca. 7 [after both base stacking and intramolecular hydrogen bonding interactions are taken into account (*25*, *26*)], the absence of a large change in rate for $\tau 1$ or $\tau 2$ in the pH range of 4.5−

8.0 is somewhat surprising. One possible explanation is that the pK_a at N-7 is perturbed to a value higher than 7. It should be noted that if there is a change in the rate-determining step at high pH, then intrinsic pK_a values may also be perturbed to higher values, giving larger apparent pK_a values (*43*). A kinetic pK_a effect is predicted in Scheme 2 in the event that the rate of chemistry (τ1 or k_3) decreases at high pH; unfortunately, the pH dependency of τ1 was not measurable above pH 8.0, so this prediction remains to be tested.

Alternatively, the small observed pH dependencies for τ1 and τ2 may result from the presence of an isomerization step prior to chemistry that is rate-determining at all pH's (consistent with the strong temperature dependence of τ1). This explanation is incorporated into the one-chemistry step model of Scheme 2 to account for the slower apparent rate of chemistry during τ2. Rate-determining conformational changes that precede chemistry have been observed in other enzymes, for example, DNA polymerase (*44*), and can often be detected using fluorescence spectroscopy. However, no fluorescence transients with rate constants corresponding to those of τ1 were observed. Thus, as yet, there is no evidence for a rate-limiting conformational change for τ1.

A final explanation for the weak pH dependencies is that protonation of the leaving group is not catalytic. This explanation is consistent with the proposal that the proton donor of the leaving group is solvent (as is likely; see the introductory section). It should also be noted that it is unlikely that buffer acts as the proton donor at N-7: dilution of the buffer either had no effect on burst rates (for phosphate buffer, in the range of 0.1−100 mM) or had a stimulatory effect as a result of buffer inhibition (for amine buffers; see Materials and Methods).

The Rate of Base Release Is Determined by a Prior Step. The failure to observe mixed product inhibition sets a lower limit (>600 μM) for the dissociation constant of the base from the E·ribose·base complex. As small molecules bind to active sites with rate constants (k_{on}) typically on the order of 1−100 μM^{-1} s^{-1} at 25 °C (*45*), it follows that k_{off} for base dissociation is minimally 6×10^2 to 6×10^4 s^{-1}, 2 orders of magnitude greater than the saturating rate constant for τ4. This apparent inconsistency can be explained if the rate of purine release is determined by a slower, optically transparent step that precedes the dissociation step. One candidate for this step is chemistry itself (k_3/k_4 and k_{11}/k_{12}, Scheme 2; k_3/k_4 and k_3'/k_4', Scheme 3). Alternatively, a slow isomerization event (k_{15}, Schemes 2 and 3) may occur between chemistry and base release which would give a single rate of base release. Given that active site loop movement takes place upon inhibitor binding, resulting in partial burial of the purine moiety from bulk solvent (*24*), a plausible candidate for the isomerization step is the conversion of the closed active site conformation to the open state.

In the first interpretation (chemistry being rate-determining), there ought to be two rates of base release with rate constants corresponding to those of τ1 and τ2 because there are two apparent rates of chemistry. Although clear evidence for biphasic fluorescence recovery during τ4* was not obtained, this interpretation is supported by the observation that the rate constant for τ4* was substantially greater than that of τ2 at pH 7.0 (where the amplitude of τ2 is small) but equal to τ2 at pH's where the amplitude of τ2 is larger (i.e., τ4* may represent an average of two base release transients whose rates are limited by τ1 and τ2).

In the second interpretation (isomerization being rate-determining), a single rate of base release will be apparent only if the rate of isomerization is slower than both τ1 and τ2. However, at pH 7.0, the rate of τ4* is greater than the rate of τ2, and therefore, a biphasic fluorescence recovery should also be apparent. In this case, τ4* may represent an average of two base release transients that are limited by τ2 and the isomerization step.

Reversibility of Chemistry on the Enzyme. On-the-enzyme chemistry is known to be irreversible for *Cf*NH (*18*). This is because kinetic isotope effects are fully expressed and the ratio $V_{max,forward}/V_{max,reverse}$, calculated using the kinetic Haldane relationship for a rapid equilibrium random uni-bi mechanism, is large. For *Tv*NH, the extent of reversibility for on-the-enzyme chemistry remains to be established, and therefore, forward and reverse rate constants are included in Schemes 2 and 3. It should be noted that the observation of approximate full-sites activity could potentially be caused by fast base release, rather than irreversible chemistry. Estimates of the reversibility for *Tv*NH can be made using the Haldane relationship as follows. For an ordered uni-bi mechanism, the kinetic Haldane is (*43*)

$$K_{eq} = [(k_{cat}/K_m)_{forward}K_{ribose}]/(k_{cat}/K_m)_{reverse} = [(k_{cat}/K_m)_{forward}K_{m,hyp}K_{ribose}]/k_{cat,reverse}$$

where K_{ribose} is the ribose dissociation constant and $K_{m,hyp}$ is the Michaelis constant for hypoxanthine in the reverse direction. Using this relationship, $(k_{cat}/K_m)_{reverse}$ is calculated to be 10^5-fold slower than $(k_{cat}/K_m)_{forward}$ [on the basis of a K_{eq} of 106 M (*18*), K_{ribose} = 1 mM]. An estimate for $k_{cat,reverse}$ at 25 °C can be made using the observed $(k_{cat}/K_m)_{forward}$ (1 μM^{-1} s^{-1}) and an assumed value for $K_{m,hyp}$ (which we were unable to measure): when $K_{m,hyp}$ = 100 mM, $k_{cat,reverse}$ = 1 s^{-1}. Even with such a high value of $K_{m,hyp}$, this rate is much slower than the forward rate of chemistry at 25 °C (estimated to be ca. 270 s^{-1} at 50 μM guanosine from an Arrhenius plot; data not shown), consistent with irreversible chemistry. However, whether $k_{cat,rev}$ actually represents chemistry has yet to be determined.

Conclusions and Implications for Future Studies. The assignment of transients corresponding to binding, chemistry, and base release and the development of two new kinetic models should facilitate future mechanistic studies by permitting the effects of mutagenesis on these processes to be examined. For example, the effect of mutagenesis on *Tv*NH activity can be reassessed with the discovery that the rate of chemistry (120 s^{-1} at pH 8.0) is ca. 3000 times faster than k_{cat} at 5 °C. New questions also arise from consideration of the two proposed kinetic models, namely, the role of active site loop movements in the enzyme mechanism, the identities of the two *Tv*NH·substrate complexes (syn−anti substrate conformations?), the nature of the two observed rates of chemistry (intrinsic rates?), and the origin of the slow base and ribose release (loop 2 conformation change?). Finally, the mechanism of leaving group activation, and other mechanistic aspects of *N*-glycosidic bond cleavage, require further investigation in light of the observation that the two rates of chemistry exhibit weak pH dependencies.

ACKNOWLEDGMENT

We thank Professor Michael Toney (University of California, Davis, CA) and Drs. Corinne Lionne and Tom Barman (Université Montpellier, Montpellier, France) for advice on rapid quench and Dr. Serge Chesnov of the Functional Genomics Center (Zurich, Switzerland) for the mass analyses of *Tv*NH. The rapid quench was kindly lent by Dr. André Matagne (University of Liège, Liège, Belgium).

SUPPORTING INFORMATION AVAILABLE

Discussion of the alternative model for the origin of the transient $\tau 1$ and $\tau 2$ involving a single rate of chemistry. This material is available free of charge via the Internet at http://pubs.acs.org.

REFERENCES

1. Stivers, J. T., and Jiang, Y. L. (2003) A mechanistic perspective on the chemistry of DNA repair glycosidases, *Chem. Rev. 103*, 2729−2759.
2. Krueger, K. M., and Barbieri, J. T. (1995) The family of bacterial ADP-ribosylating exotoxins, *Clin. Microbiol. Rev. 8*, 34−47.
3. Hammond, D. J., and Gutteridge, W. E. (1984) Purine and pyrimidine metabolism in the *Trypanosomatidae*, *Mol. Biochem. Parasitol. 13*, 243−261.
4. Garrett, E. R., and Mehta, P. J. (1972) Solvolysis of adenine nucleosides II. Effects of sugars and adenine substituents on alkaline solvolyses, *J. Am. Chem. Soc. 94*, 8542−8547.
5. Lindahl, T. (1993) Instability and decay of the primary structure of DNA, *Nature 362*, 709−715.
6. Horenstein, B. A., and Schramm, V. L. (1993) Electronic nature of the transition state for nucleoside hydrolase. A blueprint for inhibitor design, *Biochemistry 32*, 7089−7097.
7. Versées, W., and Steyaert, J. (2003) Catalysis by nucleoside hydrolases *Curr. Opin. Struct. Biol. 13*, 731−738.
8. Giabbai, B., and Degano, M. (2004) Crystal structure to 1.7 Å of the *Escherichia coli* pyrimidine nucleoside hydrolase YeiK, a novel candidate for cancer gene therapy, *Structure 12*, 739−749.
9. Schramm, V. L. (2003) Enzymatic transition state poise and transition state analogues, *Acc. Chem. Res. 36*, 588−596.
10. Berti, P. J., and Tanaka, K. S. E. (2002) Transition state analysis using multiple kinetic isotope effects: Mechanisms of enzymatic and non-enzymatic glycoside hydrolysis and transfer, *Adv. Phys. Org. Chem. 36*, 239−314.
11. Miles, R. W., Tyler, P. C., Evans, G. B., Furneaux, R. H., Parkin, D. W., and Schramm, V. L. (1999) Iminoribitol transition state analogue inhibitors of protozoan nucleoside hydrolases, *Biochemistry 38*, 13147−13154.
12. Degano, M., Almo, S. C., Sacchettini, J. C., and Schramm, V. L. (1998) Trypanosomal nucleoside hydrolase. A novel mechanism from the structure with a transition-state inhibitor, *Biochemistry 37*, 6277−6285.
13. Versées, W., Decanniere, K., Pellé, R., Depoorter, J., Brosens, E., Parkin, D. W., and Steyaert, J. (2001) Structure and function of a novel purine specific nucleoside hydrolase from *Trypanosoma vivax*, *J. Mol. Biol. 307*, 1363−1379.
14. Muzzolini, L., Versées, W., Tornaghi, P., Van Holsbeke, E., Steyaert, J., and Degano, M. (2006) New insights into the mechanism of nucleoside hydrolases from the crystal structure of the *Escherichia coli* YbeK protein bound to the reaction product, *Biochemistry 45*, 773−782.
15. Shapiro, R., and Kang, S. (1969) Uncatalyzed hydrolysis of deoxyuridine, thymidine, and 5-bromodeoxyuridine, *Biochemistry 8*, 1806−1810.
16. Zoltewicz, J. A., Clark, D. F., Sharpless, T. W., and Grahe, G. (1970) Kinetics and mechanism of the acid-catalysed hydrolysis of some purine nucleosides, *J. Am. Chem. Soc. 92*, 1741−1750.
17. Garrett, E. R., and Mehta, P. J. (1972) Solvolysis of adenine nucleosides. I. Effects of sugars and adenine substituents on acid solvolysis, *J. Am. Chem. Soc. 94*, 8532−8540.
18. Parkin, D. W., Horenstein, B. A., Abdulah, D. R., Estupiñán, B., and Schramm, V. L. (1991) Nucleoside hydrolase from *Crithidia fasciculate*. Metabolic role, purification, specificity, and kinetic mechanism, *J. Biol. Chem. 266*, 20658−20665.
19. Radzicka, A., and Wolfenden, R. (1995) A proficient enzyme, *Science 267*, 90−93.
20. Gopaul, D. G., Meyer, S. L., Degano, M., Sacchettini, J. C., and Schramm, V. L. (1996) Inosine-uridine nucleoside hydrolase from *Crithidia fasciculata*. Genetic characterization, crystallization, and identification of histidine 241 as a catalytic site residue, *Biochemistry 35*, 5963−5970.
21. Mazella, L. J., Parkin, D. W., Tyler, P. C., Furneaux, R. H., and Schramm, V. L. (1996) Mechanistic diagnoses of N-ribohydrolases and purine nucleoside phosphorylases, *J. Am. Chem. Soc. 118*, 2111−2112.
22. Parkin, D. W., Limberg, G., Tyler, P. C., Furneaux, R. H., Chen, X.-Y., and Schramm, V. L. (1997) Isozyme-specific transition state inhibitors for the trypanosomal nucleoside hydrolases, *Biochemistry 36*, 3528−3534.
23. Versées, W., Decanniere, K., Van Holsbeke, E., Devroede, N., and Steyaert, J. (2002) Enzyme−substrate interactions in the purine-specific nucleoside hydrolase from *Trypanosoma vivax*, *J. Biol. Chem. 277*, 15938−15946.
24. Versées, W., Barlow, J. N., and Steyaert, J. (2006) Transition-state complex of the purine-specific nucleoside hydrolase of *T. vivax*: Enzyme conformational change and implications for catalysis, *J. Mol. Biol*. (in press).
25. Versées, W., Loverix, S., Vandemeulebroucke, A., Geerlings, P., and Steyaert, J. (2004) Leaving group activation by aromatic stacking: An alternative to general acid catalysis, *J. Mol. Biol. 338*, 1−6.
26. Loverix, S., Geerlings, P., McNaughton, M., Augustyns, K., Vandemeulebroucke, A., Steyaert, J., and Versées, W. (2005) Substrate-assisted leaving group activation in enzyme-catalyzed N-glycosidic bond cleavage, *J. Biol. Chem. 280*, 14799−14802.
27. Vandemeulebroucke, A., Versées, W., De Vos, S., Van Holsbeke, E., and Steyaert, J. (2003) Pre-steady-state analysis of the nucleoside hydrolase of *Trypanosoma vivax*. Evidence for half-the-sites reactivity and rate-limiting product release, *Biochemistry 42*, 12902−12908.
28. Hiromi, K. (1979) *Kinetics of Fast Enzyme Reactions*, John Wiley & Sons, New York.
29. Dunn, D. B., and Hall, R. H. (1970) Purines, pyrimidines, nucleotides and oligonucleotides, in *CRC Handbook of Biochemistry* (Sober, H. A., Ed.) 2nd ed., pp G1−G238, CRC Press, Boca Raton, FL.
30. Cornish-Bowden, A. (1995) *Fundamentals of Enzyme Kinetics*, Portland Press, London.
31. Kuzmic, P. (1996) Program DYNAFIT for the analysis of enzyme kinetic data: Application to HIV protease, *Anal. Biochem. 237*, 260−273.
32. Eccleston, J. F., Hutchinson, J. P., and White, H. D. (2001) Stopped-flow techniques, in *Protein−Ligand Interactions: Structure and Spectroscopy* (Harding, S. E., and Chowdhry, B. Z., Eds.) pp 201−237, Oxford University Press, New York.
33. Tonomura, B., Nakatani, H., Ohnishi, M., Yamaguchi-Ito, J., and Hiromi, K. (1978) Test reactions for a stopped-flow apparatus, *Anal. Biochem. 84*, 370−383.
34. Fersht, A. (1999) *Structure and Mechanism in Protein Science*, W. H. Freeman and Co., New York.
35. Spies, M. A., Woodward, J. J., Watnik, M. R., and Toney, M. D. (2004) Alanine racemase free energy profiles from global analyses of progress curves, *J. Am. Chem. Soc. 126*, 7464−7475.
36. Parkin, D. W. (1996) Purine-specific nucleoside N-ribohydrolase from *Trypanosoma brucei brucei*, *J. Biol. Chem. 271*, 21713−21719.
37. Cleland, W. W. (1970) Steady-state kinetics, *Enzymes 2*, 1−65.
38. Foloppe, N., and Nilsson, L. (2005) Towards a full characterization of nucleic acid components in aqueous solution: Simulations of nucleosides, *J. Phys. Chem. B 109*, 9119−9131.
39. Mazumder-Shivakumar, D., and Bruice, T. C. (2005) Computational study of IAG-nucleoside hydrolase: Determination of the preferred ground state conformation and the role of active site residues, *Biochemistry 44*, 7805−7817.

40. Northrop, D. B. (1999) Rethinking fundamentals of enzyme action, *Adv. Enzymol. 73*, 25−55.
41. Kampf, G., Kapinos, L. E., Griesser, R., Lippert, B., and Sigel, H. (2002) Comparison of the acid−base properties of purine derivatives in aqueous solution. Determination of intrinsic proton affinities of various basic sites, *J. Chem. Soc., Perkin Trans. 2*, 1320−1327.
42. Stoychev, G., Kierdaszuk, B., and Shugar, D. (2002) Xanthosine and xanthine: Substrate properties with purine nucleoside phosphorylase and relevance to other enzyme systems, *Eur. J. Biochem. 269*, 4048−4057.
43. Cleland, W. W. (1990) Steady-state kinetics, *Enzymes 14*, 99−158.
44. Joyce, C. M., and Benkovic, S. J. (2004) DNA Polymerase Fidelity: Kinetics, Structure, and Checkpoints, *Biochemistry 43*, 14317−14324.
45. Eigen, M., and Hammes, G. G. (1963) Elementary steps in enzyme reactions (as studied by relaxation spectrometry), *Adv. Enzymol. 25*, 1−38.

BI060666R